

Iron-Containing Abdominal Pathologies: Exploiting Magnetic Susceptibility Artifact on Dual-Echo Gradient-Echo Magnetic Resonance Imaging

Aaron J. Thomas, MD,* Ajaykumar C. Morani, MD, MBBS, DNB,† Peter S. Liu, MD,‡
William J. Weadock, MD,§ Hero K. Hussain, MD,|| and Khaled M. Elsayes, MD†

Abstract: A multitude of pathologic entities involve abnormal iron deposition in the abdomen. These lesions demonstrate decreased signal on longer magnetic resonance sequences with longer echo time due to T2* effect. Dual-echo gradient-echo sequences demonstrate increased susceptibility artifact with longer echo sequences. In this article, the spectrum of iron-containing abdominal pathologies is illustrated, with their characteristic distributions. Included is a brief discussion of the physics of magnetic resonance imaging of iron-containing lesions.

Key Words: abdomen, hemochromatosis, hemorrhage, iron, MRI

(*J Comput Assist Tomogr* 2019;43: 165–175)

The majority of iron in the body is functional in the form of hemoglobin in red blood cells and erythroid precursors, with smaller amounts in myoglobin found in muscle, and in various enzymes such as the cytochromes. Additional iron is stored within hepatocytes and in the reticuloendothelial (RE) cells of the liver, spleen, and bone marrow.¹ Excess iron in the body can result from either excess gastrointestinal absorption or recurrent blood transfusions. Excess iron absorption from the gastrointestinal tract may be due to a variety of causes including excess ingestion, a genetic predisposition such as primary hemochromatosis, conditions causing ineffective erythropoiesis (eg, thalassemia major, sideroblastic anemia), or a combination of the above.²

The distribution of iron varies based on the mechanism of iron deposition and can be indicative of a particular pathology. For example, there is renal deposition in paroxysmal nocturnal hemoglobinuria (PNH), hepatic and renal deposition in other intravascular hemolytic disorders, and deposition in the liver and spleen in extravascular hemolytic diseases. Primary hemochromatosis and secondary hemochromatosis also have characteristic distributions that can differentiate the 2 disorders. Iron can also occur focally because of hemorrhage or other processes.³

Iron-containing pathology can be seen as focal regions of signal loss on magnetic resonance imaging (MRI) when gradient-echo (GRE) sequences are used because of inhomogeneities in the static magnetic field resulting from the paramagnetic effect of iron. This is due to the unpaired electrons of the iron-containing heme porphyrin ring in hemoglobin

degradation products (eg, deoxyhemoglobin, methemoglobin, and hemosiderin), resulting in dipole-dipole interactions, and the resulting signal loss is known as magnetic susceptibility artifact.⁴ The artifact becomes more prominent with increasing magnetic field strength,⁵ as well with increased echo time (TE).^{6,7}

IRON ON GRADIENT ECHO SEQUENCES

Magnetic susceptibility from iron is due to the paramagnetic properties from unpaired electrons resulting in the significant reduction of T2 and T2* relaxation times.⁴ Because of this, MRI can be a useful noninvasive imaging modality for the depiction of iron overload and its anatomical distribution. This T2* decay is further increased due to spin-spin interactions and magnetic field inhomogeneity, and iron-containing pathology becomes increasingly apparent with increasing TE on gradient sequences⁷ (Figs. 1, 2). This phenomenon can be exploited to characterize iron-containing entities on dual-echo GRE, which is part of standard abdominal MRI protocols.

A potential pitfall to be aware of is that other entities, such as metallic objects, air, and calcium, can exhibit loss of signal intensity with increased TE as well.^{6,7}

Dual-echo GRE sequences are already used to diagnose lipid-containing pathology due to phase cancellation effects (Fig. 3). This results from the difference in the precessional frequencies of fat and water, approximately 220 Hz at 1.5 T and approximately 440 Hz at 3.0 T. It depends on the TE, and it is seen on GRE images because the signals of water and fat are alternately summed on in-phase (IP) images and subtracted on out-of-phase (OP) images. The OP sequences occur when the TE is an odd multiple of 2.2 milliseconds on 1.5-T magnets or an odd multiple of 1.1 milliseconds on 3.0-T magnets.^{6–8} Phase cancellation is otherwise not seen on the standard SE sequences, as these have 1 or more refocusing radiofrequency pulses, making water and fat signals in phase regardless of the TE.^{6,7} Although phasicity and susceptibility effects can be exploited on dual-echo GRE to diagnose lipid- and fat-containing pathologies, increasing TE itself can decrease the signal throughout the slice in all the tissues irrespective of iron or fat content. Hence, OP and IP should be acquired with the shortest TE possible. In addition, OP images should be acquired before IP images in dual-echo GRE to be able to exploit the variable TE effects on both phase cancellation and magnetic susceptibility and distinguish between fat- and iron-containing entities at the same time with a single sequence. If not used appropriately, this can lead to pitfalls and misinterpretations.

Pitfall on 3.0-T Systems

Some 3.0-T gradient coils are not capable of achieving a short TE of 1.1 milliseconds. Thus, the initial desired OP echo at 1.1-millisecond TE and the sequential IP and OP echoes at intervals of 1.1 milliseconds cannot be acquired. Therefore, the first possible TE for these machines to acquire images for dual-echo

From the *Department of Radiology, Baylor College of Medicine; and †Department of Radiology, The University of Texas MD Anderson Cancer Center, Houston, TX; ‡Department of Radiology, Cleveland Clinic, Cleveland, OH; §Department of Radiology, University of Michigan, Ann Arbor, MI; and ||Department of Radiology, American University of Beirut, Beirut, Lebanon.
Received for publication July 30, 2018; accepted August 16, 2018.

Correspondence to: Ajaykumar C. Morani, MD, MBBS, DNB, Department of Radiology, The University of Texas MD Anderson Cancer Center, 1515 Holcombe Blvd, Unit 1473 Houston, TX 77030 (e-mail: amorani@mdanderson.org).

The authors declare no conflict of interest.

Copyright © 2018 Wolters Kluwer Health, Inc. All rights reserved.

DOI: 10.1097/RCT.0000000000000808

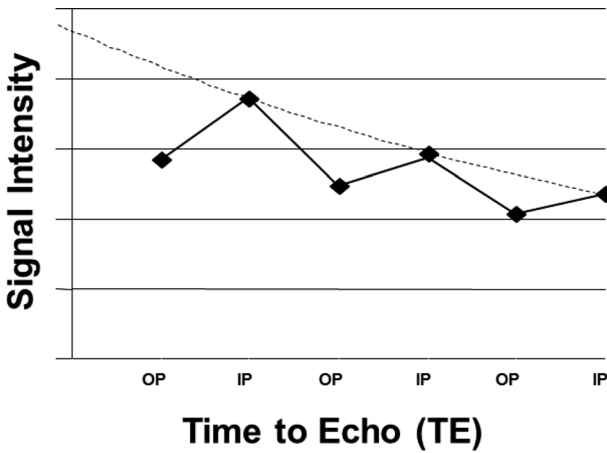


FIGURE 1. On dual-echo GRE sequences, signal intensity in iron-containing pathology decreases with increasing TE due to increased magnetic susceptibility artifact (dotted line), in addition to the phase-related signal changes (solid line).

GRE is at a TE of 2.2 milliseconds, which is IP. They also cannot acquire the next possible OP images at TE of 3.3 milliseconds because of the short interval. A potential solution is for 2 separate pulse sequences with separate breath holds to be acquired at a TE of 2.2 milliseconds (IP) and 3.3 milliseconds (OP). Because the OP image is acquired at a TE longer than the IP image, the

resulting images will suffer from a combination of chemical shift effects and increased magnetic susceptibility effects. This decreases the utility of dual-echo GRE sequences in distinguishing lipid from iron in a tissue. Also because of the separate pulse sequence required with this approach, imaging times will be longer, and image quality may suffer from misregistration artifacts.^{6,9}

For practical purposes, because of the disadvantages with separate breath holds, if a dual-echo GRE approach is to be used on a slower 3.0-T magnet, the OP acquisition is feasible only at or after a TE of 5.5 milliseconds, following acquisition of the IP image at a TE of 2.2 milliseconds. Similar to the above scenario, the resultant OP image will suffer from increased susceptibility effects due to the longer TE, again limiting the segregation of phase cancellation and magnetic susceptibility effects (Fig. 4). The prolonged TEs would also increase the imaging time.⁶ To address the issue of isolating the susceptibility from chemical shift effects, an additional possibility is an OP TE of 3.3 milliseconds followed by an IP TE of 6.6 milliseconds in dual-echo sequence. Disadvantages of this include increased imaging time and altered tissue contrast due to the prolonged TE.⁷

Radiologists should always be mindful of the TE used in a particular sequence in order to correctly distinguish iron- and fat-containing lesions. By considering the effect of the timing of the dual-echo GRE sequences on the images with respect to

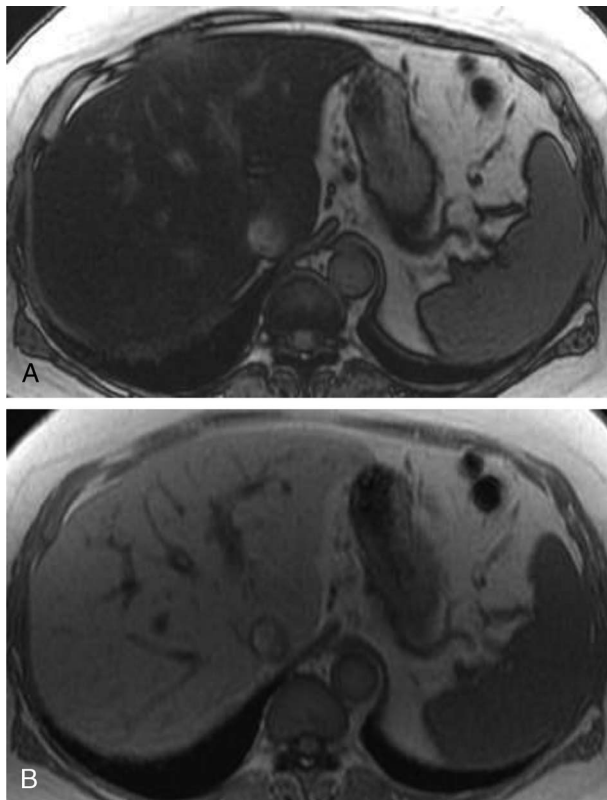


FIGURE 2. OP (A) and IP (B) GRE sequences on a 1.5-T magnet in a patient with hepatic steatosis. On OP (TE, 2.2 milliseconds) images, intravoxel water and fat protons are oppositely aligned resulting in signal loss. On IP (TE, 4.4 milliseconds) images, intravoxel water and fat protons are aligned together, resulting in additive signal.

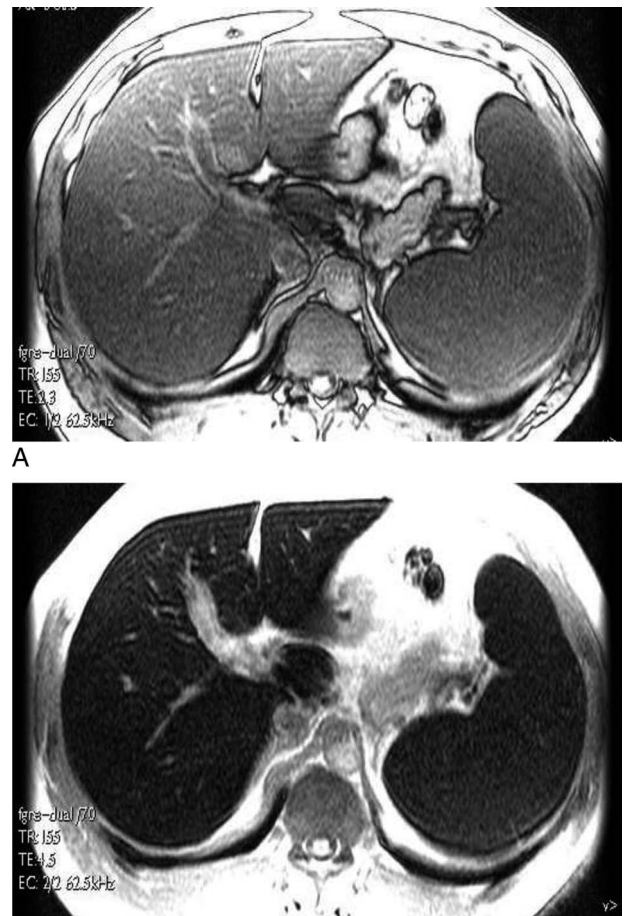


FIGURE 3. OP (TE, 2.2 milliseconds) (A) and IP (TE, 4.4 milliseconds) (B) GRE sequences on a 1.5-T magnet in a patient with hemochromatosis. Iron deposition results in decreased signal on longer TE GRE sequences due to the T2* effect.

Downloaded from http://journals.lww.com/jcat by BhDM5ePpKav1zEoum11QIN4a+kLhEzqpsIH04XW0h0CwCX1AW nYQp/IOH-D31D00dRy/ITVFA/C13V/C1Y0abgQZXdGgJ2MwZLel= on 08/07/2024

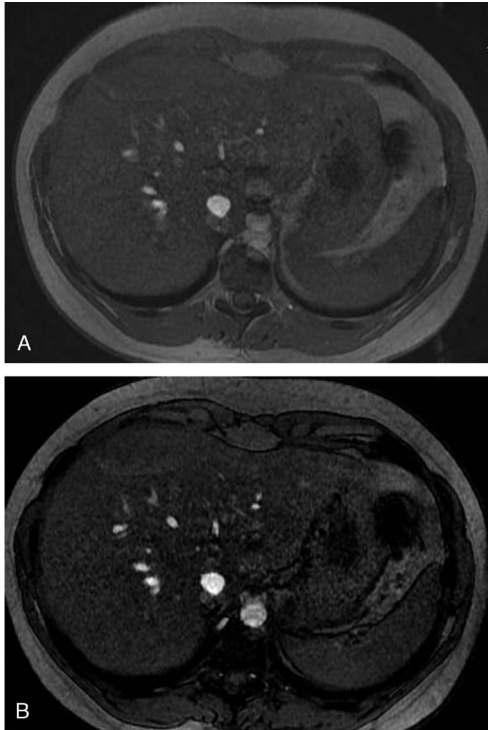


FIGURE 4. IP (A) and OP (B) sequences on a 3.0-T magnet. Because this machine cannot acquire the initial OP image at TE 1.1 milliseconds or echoes separated by only 1.1 milliseconds, the IP is acquired with TE 2.2 milliseconds, and OP is acquired at TE 5.5 milliseconds. Therefore, it cannot be determined if signal loss in the liver on OP is due to phase cancellation of fat/lipid and water or signal decay due to magnetic susceptibility related to iron on the longer TE OP image.

magnetic susceptibility and chemical shift effects, the potential limitations of the examinations in distinguishing lipid- and iron-containing pathologies can be understood, regardless of the magnetic resonance system used.

Iron in Liver

Iron deposition in the liver can be focal because of portal venous flow abnormalities or tumor, or it can be more diffuse as seen in iron overload disease, intravascular hemolysis, or cirrhosis, particularly when due to alcohol abuse. Iron deposition in patients with alcoholic cirrhosis is usually to a far lesser extent than seen in hemochromatosis.¹⁰

Hemochromatosis

Hemochromatosis refers to abnormal iron accumulation in the body and can be primary or secondary. Primary hemochromatosis is an autosomal recessive disease and affects males 10 times more frequently than females. It results from excessive intestinal absorption of iron, with excess deposition in the liver, pancreas, myocardium, endocrine glands, joints, and skin (Fig. 5).^{11–13} In contrast to the secondary form of hemochromatosis (more commonly known as hemosiderosis), primary hemochromatosis results in iron deposition within the hepatocytes, typically seen earliest in the periportal regions, as iron is delivered via the portal venous system following intestinal absorption.¹³ The Kupffer cells of the liver as well as other parts of the RE system are spared.¹⁴

In contrast, patients with hemosiderosis due to chronic blood transfusions demonstrate primarily RE iron overload involving the Kupffer cells of the liver, with spread to surrounding hepatocytes in more advanced disease.¹⁵ Because of the predominant RE deposition, the primary affected organs are liver and spleen without extensive additional organ involvement^{13,16} (Fig. 6). Hemosiderosis most commonly results from repeated blood transfusions and can also be seen with high iron intake and

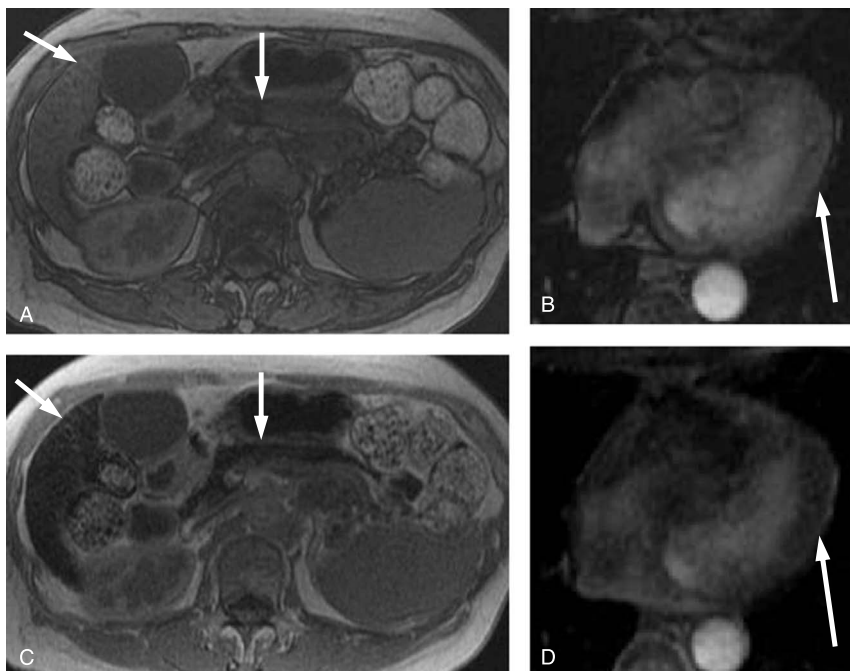


FIGURE 5. OP (TE, 2.2 milliseconds) (A, B) and IP (TE, 4.4 milliseconds) (C, D) GRE sequences of the abdomen and heart in a patient with primary hemochromatosis demonstrate decreased signal in the liver, pancreas, and myocardium (arrows) on the longer TE IP GRE sequence compared with OP because of parenchymal iron deposition. Sparing of the spleen is consistent with primary hemochromatosis.

Downloaded from http://journals.lww.com/jcat by BhDM5fPHeKAvI2Eoum11QIN4a+kLHEZp8sIH04XIM0hCwCX1AW nYQp/IOH-D3I3D00dRy/TVSFAIC3V/C1y0abgqZKdG9j2MwZLel= on 08/07/2024

underlying liver diseases such as alcoholic cirrhosis or portacaval shunts as well as hemolytic anemia. A unique form of secondary hemochromatosis is an exception to the expected distribution described above and occurs in patients with ineffective erythropoiesis due to thalassemia or sideroblastic anemia. In these cases, iron overload results from increased absorption resulting in an identical distribution to primary hemochromatosis.³

Magnetic resonance imaging demonstrates markedly decreased signal intensity in affected organs on GRE and T2-weighted images owing to the paramagnetic effects of iron.³ The main distinguishing feature of hemosiderosis is involvement of the spleen and bone marrow, which are characteristically spared in the primary form of hemochromatosis (Fig. 5).¹⁰ Hemosiderosis spares other characteristic sites seen in primary hemochromatosis such as the pancreas and myocardium, but these may not be spared in advanced cases.

In both forms of hemochromatosis, the deposited iron incites a fibrotic reaction and may lead to cirrhosis.^{13,15} Because dysplastic cells of hepatocellular carcinoma (HCC) do not accumulate iron to same extent as the liver parenchyma, any concomitant HCC will appear as a focus of high signal intensity on a background of relatively low signal intensity on gradient and T2-weighted images (Figs. 7, 8).^{13,17}

Magnetic resonance imaging is also a useful and noninvasive diagnostic tool for quantification of hepatic iron concentration.¹² Detailed description of hepatic iron quantification is beyond the scope of this article. Briefly, this can be achieved using a signal intensity ratio, where the ratio of the hepatic parenchymal signal

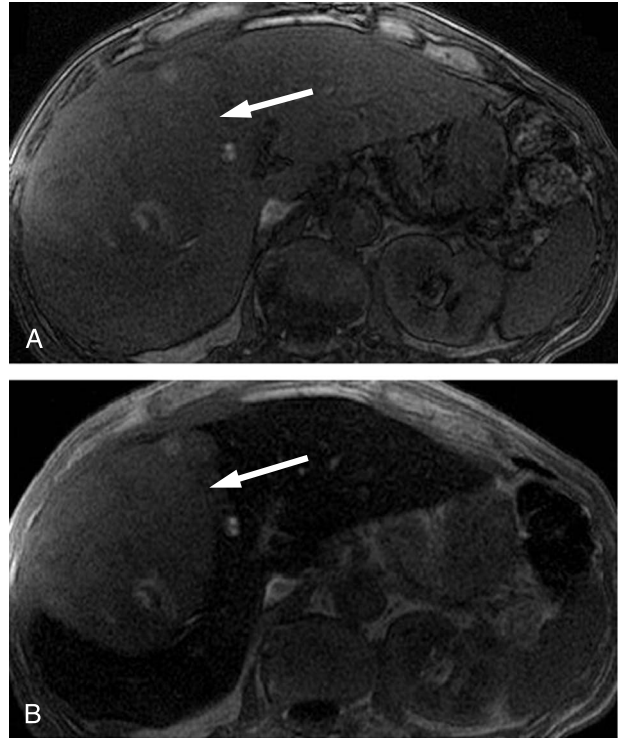


FIGURE 7. OP (TE, 2.2 milliseconds) (A) and IP (TE, 4.4 milliseconds) (B) GRE sequences demonstrates decreased hepatic signal on the longer TE sequence, consistent with hemochromatosis, with a large hyperintense hepatic lesion more apparent on the longer TE sequence (arrow) representing HCC.

compared with the adjacent skeletal muscles allows estimation of the iron content.^{15,18} Alternatively, R2 and R2* relaxometry techniques are becoming increasingly used to quantify the iron content of the liver based on the increased relaxation rates in iron-overloaded tissue over a series of images with increasing TE.¹⁹ Also, a recently developed technique known as proton density fat fraction uses chemical shift–based techniques to quantify fat and uses T2* data to correct for iron content, allowing quantification of both iron and fat independently.²⁰ Magnetic resonance imaging can be used to monitor the progression of iron deposition as well as treatment response, serving as a noninvasive alternative to serial biopsies.^{15,18,21}

Hemolytic Anemias

Hemolytic anemias can be categorized as intravascular hemolysis, occurring in the blood vessels, or extravascular, in which the red blood cells are lysed primarily in the RE system. After intravascular hemolysis, released hemoglobin binds to plasma haptoglobin, which is usually taken up by hepatocytes leading to parenchymal iron deposition, similar to primary hemochromatosis. Extravascular hemolysis occurs primarily in the macrophages of the RE system in the spleen and liver, resulting in hemosiderosis.^{3,22}

Cirrhosis

Some patients with cirrhosis who do not have genetic hemochromatosis absorb excess iron and can develop a mild form of siderosis that does not require treatment. A characteristic pattern of iron deposition surrounding the hepatic veins has been described in the setting of alcoholic cirrhosis.²³

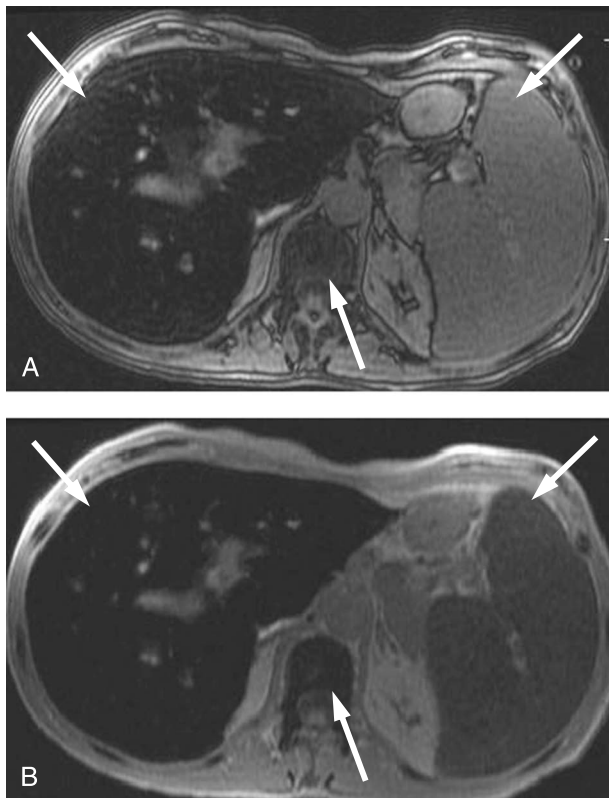


FIGURE 6. OP (TE, 2.2 milliseconds) (A) and IP (TE, 4.4 milliseconds) (B) GRE sequences in a patient with hemosiderosis demonstrates decreased signal in the liver, spleen, and bone marrow (arrows) on the longer TE T1-weighted IP image due to iron deposition resulting from recurrent blood transfusions. Splenic involvement excludes primary hemochromatosis.

Downloaded from http://jcat.org/ at BnDw5eP8Kav1Z5Eumt1QIN4a+KJLhEzpsHh4XN0hCwCX1AW on 08/07/2024

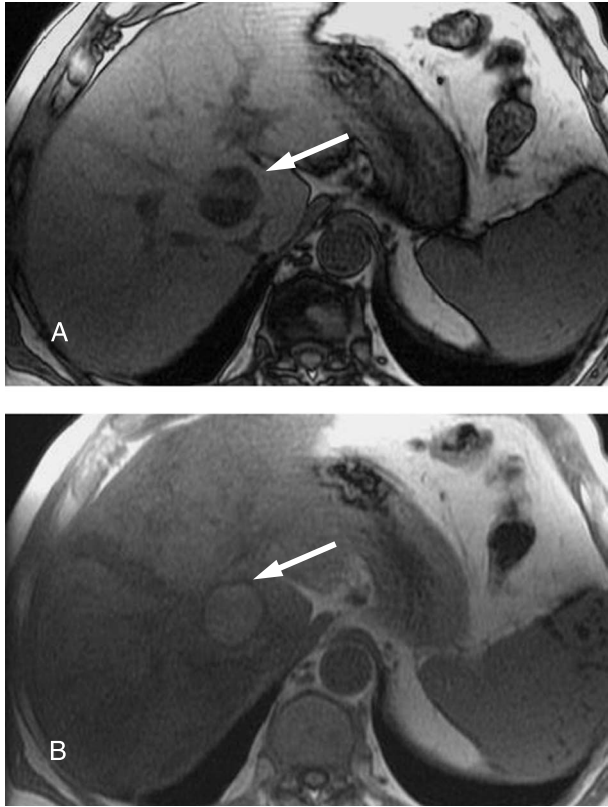


FIGURE 8. OP (TE, 2.2 milliseconds) (A) and IP (TE, 4.4 milliseconds) (B) GRE sequences through the liver in a patient with HCC demonstrate loss of signal in the mass (arrow) on OP sequence, consistent with lipid content, with heterogeneous decreased signal in the background liver on the longer TE IP image due to parenchymal iron deposition in hemochromatosis.

Siderotic Liver Nodules

Abnormal iron accumulation may develop diffusely within the hepatic parenchyma or as focally within nodules in patients with cirrhosis. Hyperactive transferrin receptor proteins may be responsible for the abnormal hepatocyte iron accumulation in these cases, resulting in iron-containing siderotic regenerative nodules. Gradient-echo pulse sequences with long TEs are an excellent modality for the detection of these lesions (Fig. 9).²⁴

It is important to distinguish siderotic from focal steatotic nodules in the liver, as isolated steatotic nodules or fatty change in a dysplastic nodule may have potential to become malignant or may indicate malignant transformation²⁴⁻²⁶ (Fig. 8). Although any lesion in the setting of hemochromatosis should be viewed with suspicion given the higher baseline risk of developing HCC, the presence of numerous steatotic nodules of less than 1 cm in diameter suggests that the lesions are benign (Fig. 10), but lesions larger than 1.5 cm or those that exhibit T1 hypointensity on IP images are suggestive of malignancy.^{25,27} By contrast, siderotic nodules are essentially always benign²⁴ except in cases of hemorrhagic tumor. Thus, the distinction between siderotic and steatotic hepatic nodules will impact the need for follow-up imaging in these cases.²⁵ To distinguish the two, dual-echo GRE can be very useful. Siderotic nodules will show drop of signal on longer TE IP images, whereas steatotic nodules will lose signal on OP images. Hence, while interpreting the hepatic lesions with focal drop of signal on

T1-weighted GRE images, not only the TE, but also phasicity of the sequences, is to be considered.

Other Focal Hepatic Iron Deposition Entities

Focal iron deposition in a segmental distribution has been reported in the liver in regions with decreased portal venous flow, resulting from portal venous compression, occlusion, or shunting.²⁸ Focal iron deposition can also be seen due to hemorrhage or hemorrhagic lesions of the liver such as hemorrhagic hepatic adenoma, HCC, metastatic melanoma, or choriocarcinoma (Fig. 11).³

Iron in Kidneys

Renal Cortical Siderosis

Intravascular hemolysis, as described above, can be seen in a wide spectrum of disorders including PNH, sickle cell disease, thalassemia, or with malfunctioning prosthetic cardiac valves. When the transport capacity of the plasma haptoglobin is exceeded, the hemoglobin released during hemolysis is filtered through renal glomeruli, reabsorbed, and stored in proximal convoluted tubules resulting in renal cortical hemosiderosis.²⁹ Thus, intravascular hemolysis leads to iron deposition in the liver and renal cortex, but not in the spleen.

In normal, well-hydrated individuals, the renal cortex appears more intense than the medulla on T1-weighted MRI scans because of its shorter T1. This normal corticomedullary

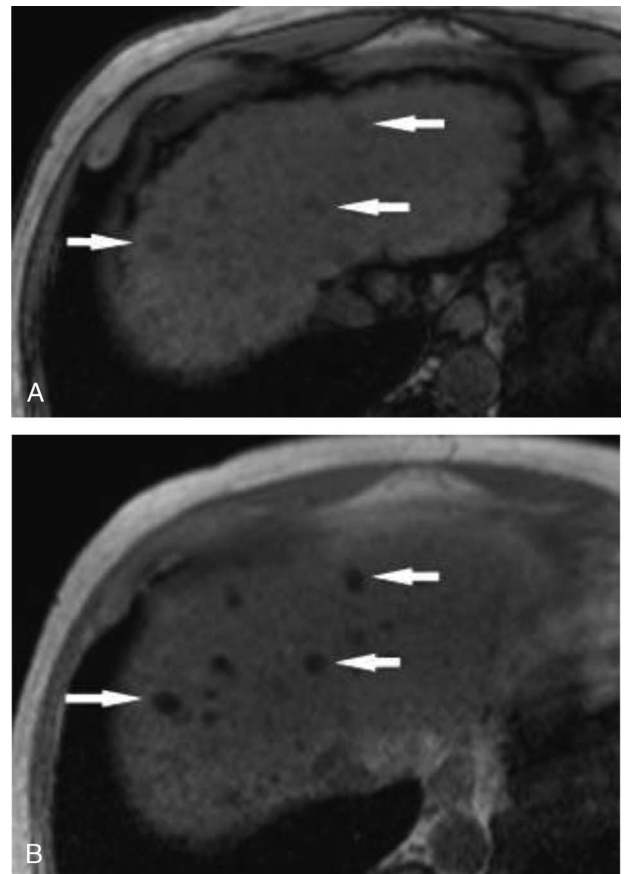


FIGURE 9. OP (TE, 2.2 milliseconds) (A) and IP (TE, 4.4 milliseconds) (B) GRE sequences in a patient with cirrhosis with multiple nodules (arrows) that demonstrate decreased signal on the longer TE IP sequence, consistent with siderotic nodules in the liver.

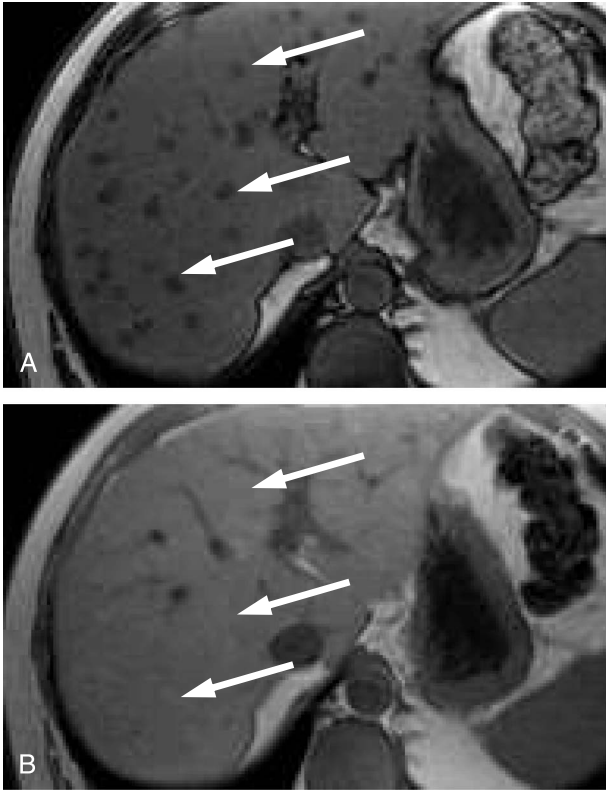


FIGURE 10. OP (TE, 2.2 milliseconds) (A) and IP (TE, 4.4 milliseconds) (B) GRE sequences demonstrate multiple nodules (arrows) with signal loss on OP images, consistent with multifocal nodular steatosis in the liver.

differentiation is lost when a disease such as iron deposition leads to isointensity of the cortex and medulla. As more iron is deposited, reversal of the normal cortical-to-medullary intensity ratio is seen on T1-weighted images and low cortical intensity on T2-weighted images due to the paramagnetic effects of iron deposited in renal cortex.^{22,30} Consequently, it will demonstrate decreased signal on longer TE images in dual-echo GRE. As mentioned previously, excess intravascular hemoglobin will also be deposited in the liver parenchyma, but spare the RE system.

An exception to this is PNH, a myelodysplastic, hematopoietic stem cell disorder, characterized by an increased complement-mediated erythrocyte lysis,³⁰ which results in relatively little liver parenchymal deposition, in contrast to other intravascular hemolytic anemias. Paroxysmal nocturnal hemoglobinuria is a chronic hemolytic anemia of unknown etiology, associated with morning hemoglobinuria, variable acholuric jaundice, and striking hemosiderinuria, all resulting from hemolysis. Hemolysis may be precipitated by infections, surgery, transfusions, drugs, immunizations, exercise, or radiographic contrast material.³¹ In PNH, there is usually absent or very little parenchymal iron deposition in the liver due to heavy renal hemoglobin deposition and urinary iron loss. There is little to no iron deposition in the liver or spleen unless there is transfusion-related hemosiderosis.²² On imaging, PNH results in enlargement of the kidneys, cortical thinning, cortical infarcts, and papillary necrosis in association with cortical iron deposition (Fig. 12).^{11,30,32}

Renal Medullary Siderosis

Uncommon compared with cortical iron deposition, hemosiderin deposition in the medulla can be from infectious or vascular causes. Hantavirus, an uncommon viral illness that results in hemorrhagic fever with renal syndrome, can result in diffuse iron accumulation within the renal medulla, especially the outer medulla. This finding, although very specific on biopsy, may be missed because of sampling error, making MRI useful for its diagnosis.³³ Acute renal venous thrombosis may result in congestion with hemorrhage and a similar appearance on imaging. In both, dual-echo GRE will show loss of signal preferentially in the outer renal medulla on the longer TE sequences.³⁴

Focal Renal Hemorrhage

A broad range of pathologies, from benign hemorrhagic cysts to neoplasms, such as angiomyolipoma or renal cell carcinoma, may display signal inhomogeneity due to iron and hemoglobin degradation products. This can occasionally provide clues to the underlying pathology, for example, in papillary renal cell carcinoma, which more commonly has internal hemosiderin compared with clear cell carcinoma. As in other iron-containing lesions, signal loss may be seen on longer TE image of dual-echo GRE sequence.²²

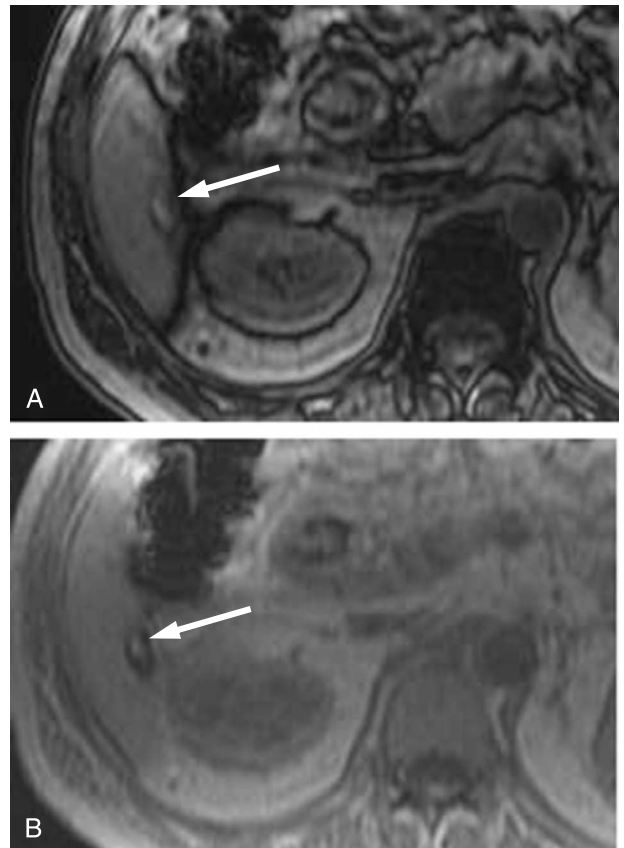


FIGURE 11. OP (TE, 2.2 milliseconds) (A) and IP (TE, 4.4 milliseconds) (B) GRE sequences demonstrate a lesion in segment 6 liver, with a peripherally hypointense rim (arrow), which shows further signal loss on the longer TE IP sequence, consistent with a hemosiderin rim in a postbiopsy hematoma.

Downloaded from http://journals.lww.com/jcat by BhDM5fPHeKav1ZEOum1QIN4a+KLLhEz9psIh64XMM0hCwCX1AW nYQp/IOHHD3I3D00dRyITVfSfACI3V/C1y0abggQZXdg9j2MwLzLeI= on 08/07/2024

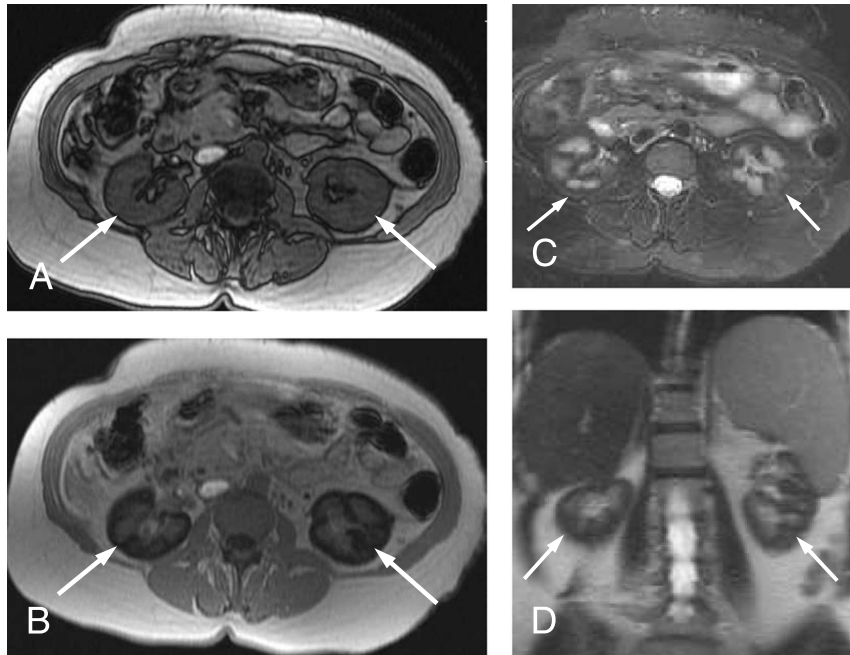


FIGURE 12. OP (TE, 2.2 milliseconds) (A) and IP (TE, 4.4 milliseconds) (B) GRE sequences in a patient with PNH show loss of signal in the renal cortex (arrows) on the longer TE IP sequence compared with the OP sequence. Note the reversal of the normal renal cortex-medulla differentiation on the IP GRE sequence. On T2-weighted sequences (C, D), the renal cortex is diffusely hypointense.

Iron in Pancreas

Diffuse iron deposition in the pancreas is typically seen in primary hemochromatosis more commonly than in hemosiderosis. In the early stages, the signal intensity of the pancreas remains

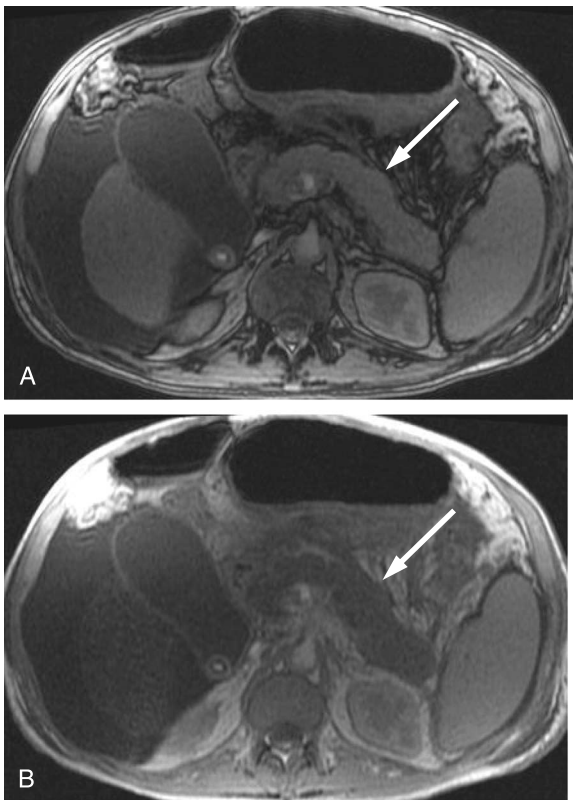


FIGURE 13. OP (TE, 2.2 milliseconds) (A) and IP (TE, 4.4 milliseconds) (B) GRE sequences in a patient with advanced primary hemochromatosis and cirrhosis demonstrate diffuse signal loss in the pancreas (arrow) on the longer TE IP sequence, representing parenchymal iron deposition.

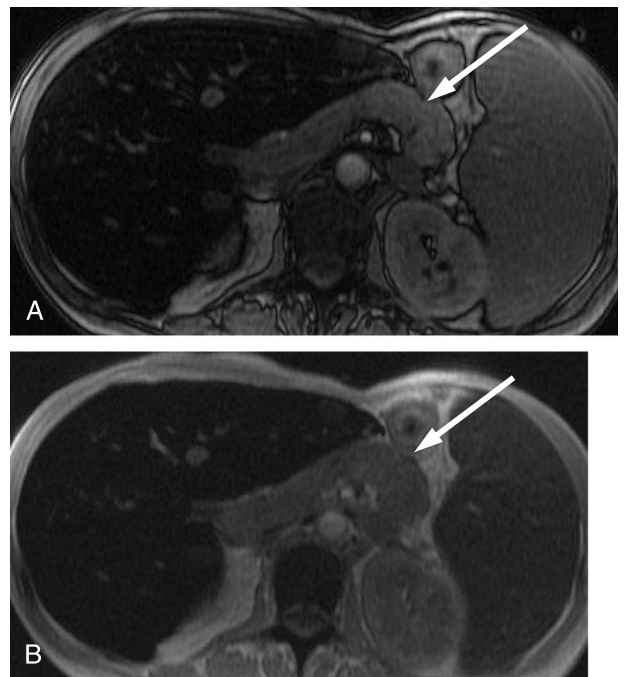


FIGURE 14. OP (TE, 2.2 milliseconds) (A) and IP (TE, 4.4 milliseconds) (B) GRE sequences in a patient with hemosiderosis due to repeated transfusion show signal loss in the pancreas (arrow), liver, and spleen on the longer TE IP sequence, representing diffuse parenchymal iron deposition.

Downloaded from http://journals.lww.com/jcat by BnDWM5eP-HKav1ZEoum1tQIN4a+kLJhEz9psiH64XIM0hCywCX1AW nYQp/IOH-D3I3D00dRy/TVSfACI3V/C1y0abggQZXdgSj2MwZLel= on 08/07/2024

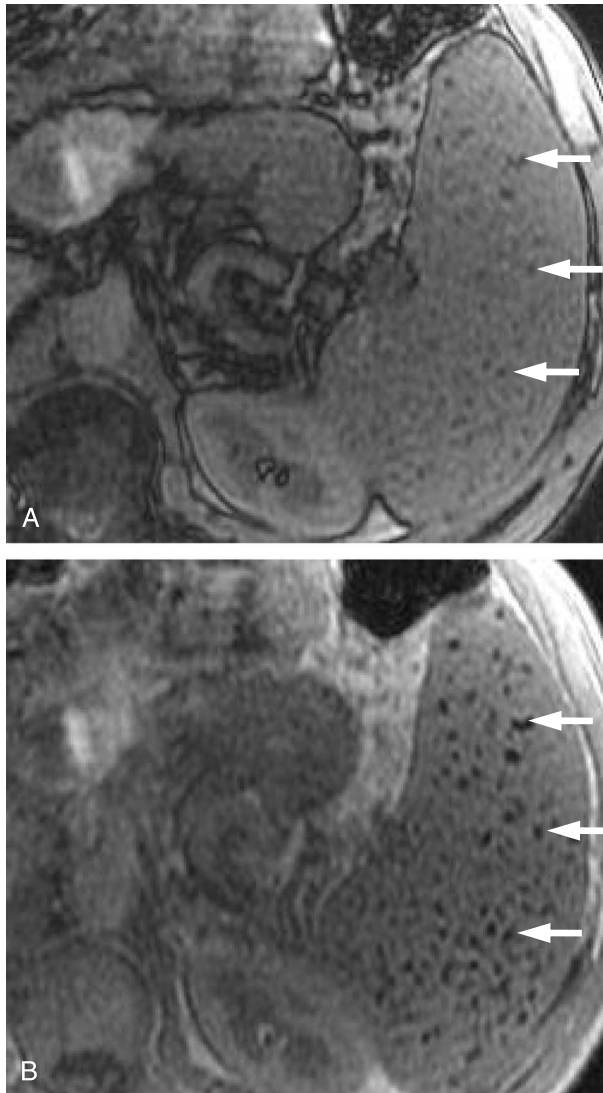


FIGURE 15. OP (TE, 2.2 milliseconds) (A) and IP (TE, 4.4 ms) (B) GRE sequences in a patient with portal hypertension show numerous foci/nodules of signal blooming (arrows) in the spleen on IP (longer TE) image compared with OP image due to susceptibility from hemosiderin within the Gamna-Gandy bodies.

normal, particularly in menstruating women. However, as the disease progresses, the signal within the pancreatic tissue decreases with increased TE, as in other involved organs (Figs. 13, 14).³⁵

Focal iron deposition may also be seen in hemorrhagic lesions of the pancreas. A wide array of neoplastic and nonneoplastic lesions can result in focal hemorrhage, including hypervascular islet cell tumors, acinar cell tumors, cystic tumors such as serous cystadenoma and solid pseudopapillary tumors, and hypervascular metastases. In addition, nonneoplastic etiologies of focal iron deposition include hemorrhagic pancreatitis, peripancreatic pseudoaneurysm, or trauma, all of which may result in focal iron deposition.³⁶

Iron in Spleen

Diffuse Distribution

Diffuse iron deposition in the spleen most commonly occurs as part of the uptake in the RE system, such as in hemosiderosis,

most commonly in the setting of chronic transfusions,³ (Fig. 6). It is also especially prominent with sickle cell disease, which results in both extravascular and intravascular hemolysis. Perivascular and parenchymal calcifications are also seen in the splenic tissue in addition to iron deposition, contributing to the diminished splenic intensity on T1- and T2-weighted images.³⁷ As discussed previously, the splenic involvement is diagnostic for hemosiderosis, and the spleen is characteristically spared in primary hemochromatosis and intravascular hemolysis.³

Focal Distribution

Focal iron deposition can be due to a number of causes. In the setting of portal hypertension, small foci of organized hemorrhages can be seen in the spleen, resulting in siderotic nodules known as Gamna-Gandy bodies. These are usually

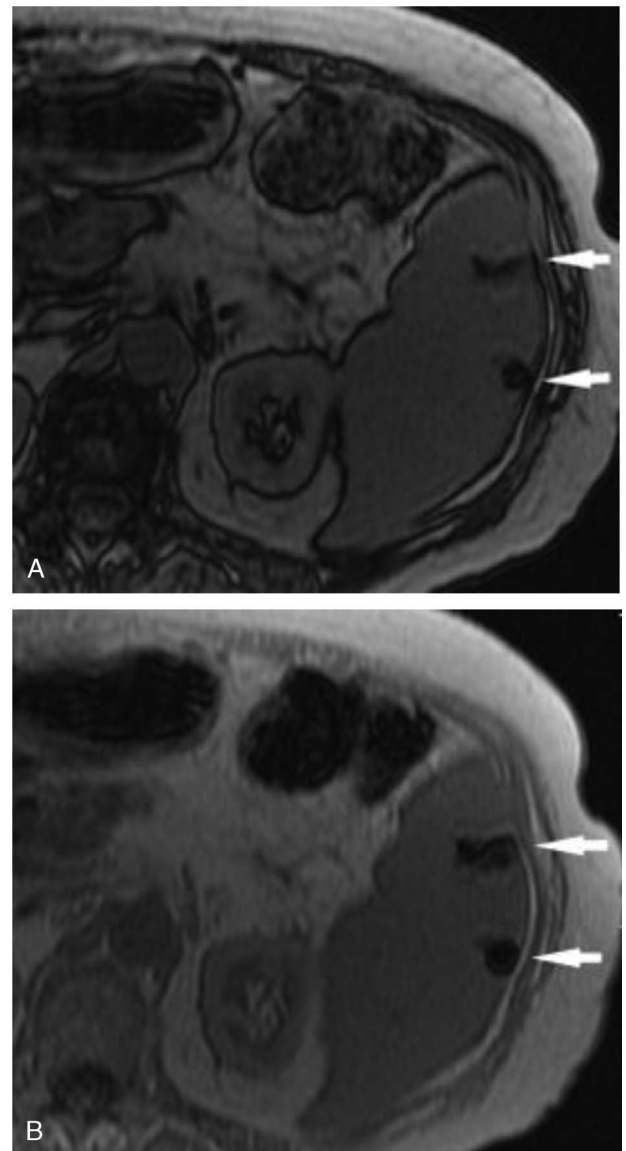


FIGURE 16. OP (TE, 2.2 milliseconds) (A) and IP (TE, 4.4 milliseconds) (B) GRE sequences show foci of blooming signal (arrows) in the old hemorrhagic infarcts in the spleen on IP (longer TE) image compared with the OP image due to susceptibility from hemosiderin.

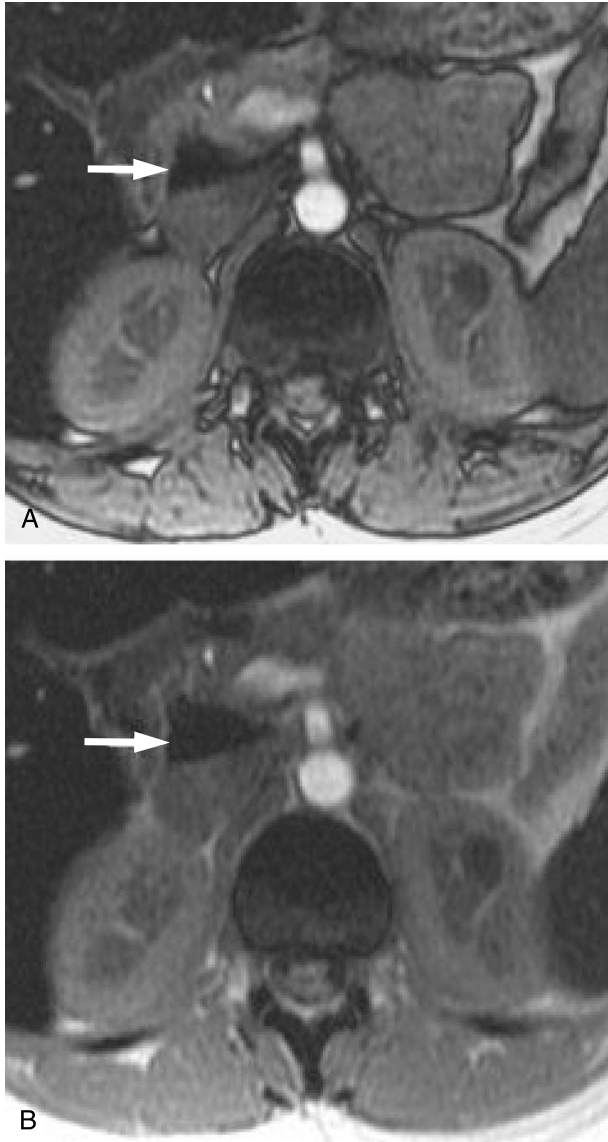


FIGURE 17. OP (TE, 2.2 milliseconds) (A) and IP (TE, 4.4 milliseconds) (B) GRE sequences in a patient with hemosiderosis demonstrate iron in a portocaval lymph node (arrow) and in the visualized liver and spleen, manifesting as signal loss on the IP (longer TE) image.

located in the perifollicular and trabecular region and are composed of fibrous tissue encrusted with hemosiderin and calcium.^{38–40} It is the iron-containing hemosiderin within these bodies that leads to susceptibility effect causing signal drop on longer TE dual-echo GRE images (Fig. 15). A potential differential diagnosis is calcified granuloma, but this does not cause blooming and may cause a very subtle change as it is diamagnetic.

Iron deposition can also be seen in the setting of vascular or hemorrhagic lesions of the spleen such as hemangioma, littoral cell angioma, angiosarcoma, or with evolving hematoma (Fig. 16). Siderotic nodules can also be seen in cases of peliosis, which usually presents in immunocompromised patients and frequently involves the liver as well. Most commonly, this disease appears as multiple cystic and hemorrhagic

nodules, which may be hypervascular and associated with the siderotic nodules.^{38,41}

Miscellaneous

Iron in the Lymph Nodes

As lymph nodes are part of the RE system, these also show iron deposition in hemosiderosis. This can be prominent enough to appear dense even on plain radiographs in advanced cases.⁴² On MRI, as in other iron-containing lesions, these will appear darker in signal intensity on longer TE IP dual-echo GRE images (Fig. 17).

Iron in Adrenal Glands

Focal signal loss within an adrenal lesion may be due to magnetic inhomogeneity resulting from iron and hemoglobin degradation products in the setting of an adrenal hematoma.⁴³ By exploiting the magnetic susceptibility effect, which is more pronounced on longer TE image, diagnosis can be made on dual-

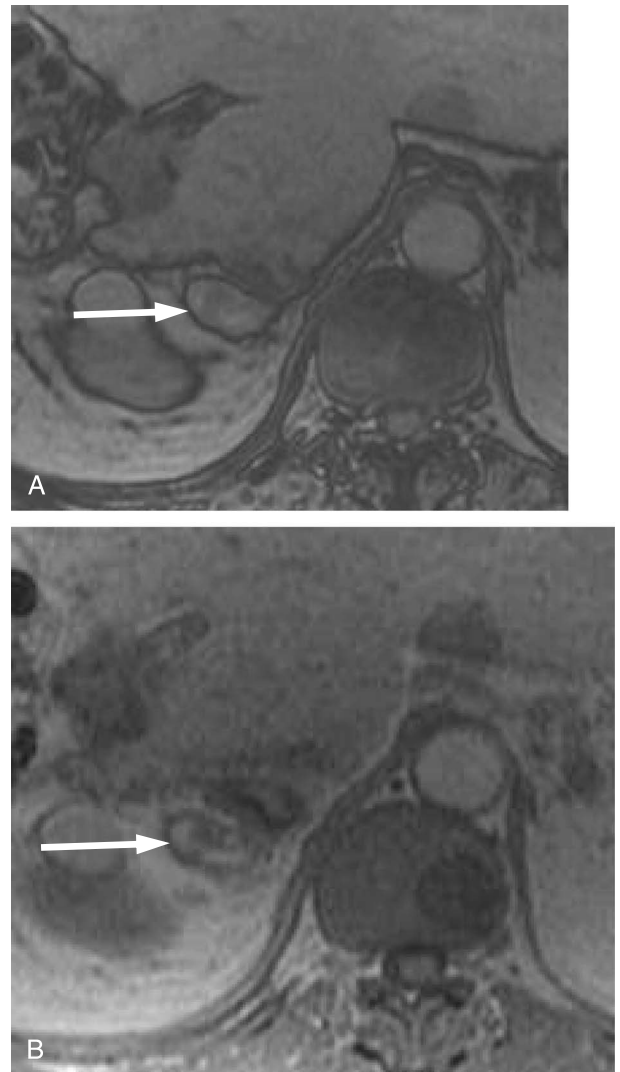


FIGURE 18. OP (TE, 2.2 milliseconds) (A) and IP (TE, 4.4 milliseconds) (B) GRE sequences demonstrate T1 heterogeneous signal in a right adrenal hematoma. Signal drop in its anterior portion on IP (longer TE) image is due to iron deposition.

echo GRE (Fig. 18). However, phasicity of the image also needs to be carefully considered while interpreting these images as previously discussed, because lipid-rich adrenal adenoma is a very common adrenal lesion that shows loss of signal on OP images (Fig. 10).⁴⁴

Diffuse adrenal iron deposition has also been described in the setting of both primary hemochromatosis and hemosiderosis, as well as in the setting of hemolysis, especially thalassemia.^{44,45} The degree of iron deposition can be quantified using the susceptibility effects in a manner similar to that in the liver^{45,46} (Fig. 19).

Iron in the Abdominal Wall

Hematomas and other hemorrhagic lesions such as endometriomas in the abdominal wall or abdominal wall hematomas resulting from trauma or other causes can sometimes be diagnosed easily on dual-echo GRE sequence, by showing signal loss within or at the periphery (hemosiderin rim) of the lesion.⁴⁷ In the case of a lesion of indeterminate origin, signal loss on long TE image suggests the iron content of these lesions and thus may help establish the diagnosis (Fig. 20).

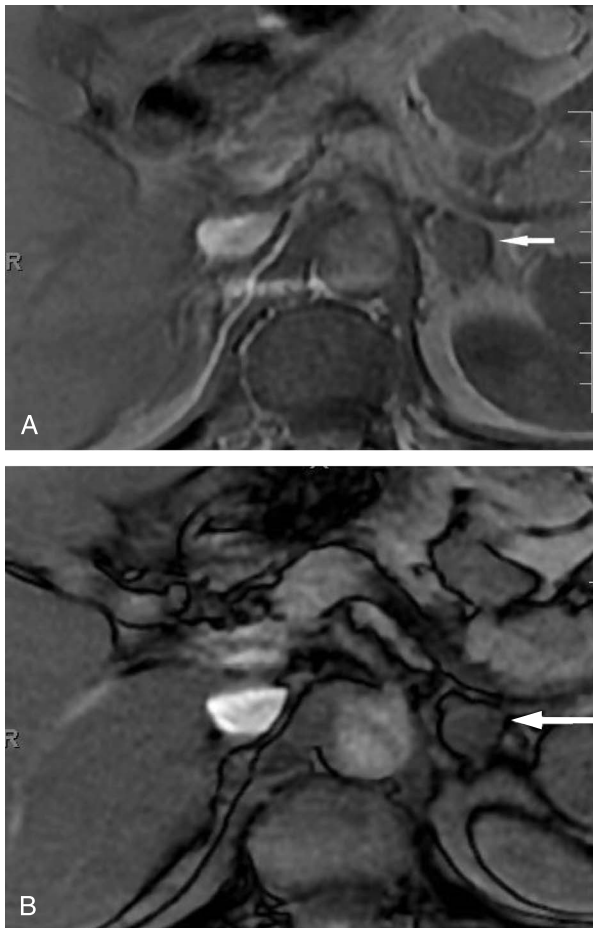


FIGURE 19. IP (TE, 2.2 milliseconds) (A) and OP (TE, 5.5 milliseconds) (B) sequences on a 3.0-T magnet demonstrate signal loss in a left adrenal nodule (arrow) on the longer TE OP image. Because the OP image was obtained at a longer TE, it cannot be determined if signal loss in the left adrenal gland is due to phase cancellation related to lipid content or magnetic susceptibility related to iron deposition or combined effects.

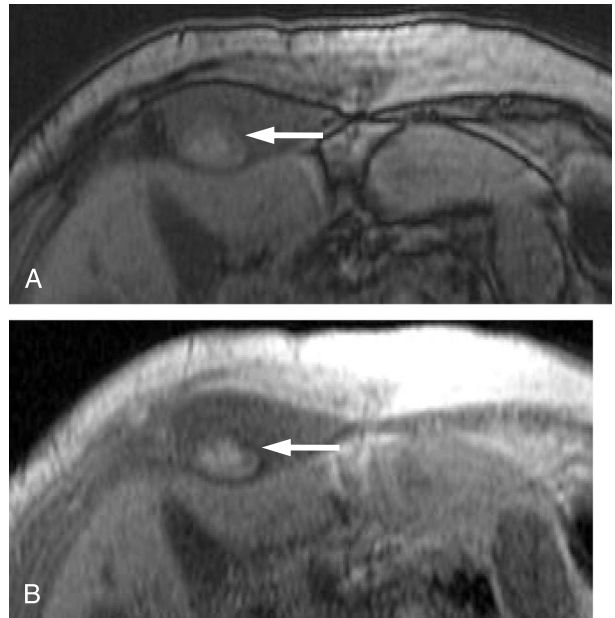


FIGURE 20. OP (TE, 2.2 milliseconds) (A) and IP (TE, 4.4 milliseconds) (B) sequences demonstrate a T1 hyperintense lesion (arrow) in right rectus abdominis with a peripheral rim of signal loss on the IP (longer TE) compared with the OP image because of hemosiderin deposition in the periphery of an evolving hematoma.

CONCLUSIONS

A broad spectrum of iron-containing abdominal pathologies can be diagnosed on dual-echo GRE by exploiting the T2* effect on the longer TE sequence. However, the OP and IP of the dual-echo GRE should be acquired with as short as possible TE, as prolonged TE itself may result in susceptibility-related signal drop irrespective of iron or fat content. At the same time, OP images should ideally be acquired before IP images in dual echo-GRE. Although there may be potential complications such as coexisting fat and iron within a lesion, this would provide better information regarding chemical shift in the image, allowing assessment of the microscopic fat content of the lesions without being affected by longer TE or magnetic susceptibility effects. This can enable us to diagnose both fat- and iron-containing abdominal entities by exploiting the variable TE and its effects on both chemical shift and magnetic susceptibility effects in a single dual-echo GRE sequence. This may be a challenge on some slower 3.0-T magnetic resonance systems, on which OP TE is longer than IP TE, or otherwise IP TE is acquired at a very prolonged TE in order to acquire OP at early TE. The result is that the signal drop on dual-echo GRE in such cases can potentially be due to multiple factors in different combinations leading to misinterpretations. Irrespective of the magnet type, if the dual-echo GRE is not acquired or used appropriately, this can lead to pitfalls and to misdiagnosis as discussed previously. The correct interpretation of the dual-echo GRE sequences in combination with knowledge of the characteristic distribution of iron in various organs as discussed can often lead to the correct diagnosis.

REFERENCES

1. Andrews NC. Disorders of iron metabolism. *N Engl J Med.* 1999;341: 1986–1995.
2. Pomerantz S, Siegelman ES. MR imaging of iron depositional disease. *Magn Reson Imaging Clin N Am.* 2002;10:105–120. vi.

3. Siegelman ES, Mitchell DG, Semelka RC. Abdominal iron deposition: metabolism, MR findings, and clinical importance. *Radiology*. 1996; 199:13–22.
4. Parizel PM, Makkat S, van Miert E, et al. Intracranial hemorrhage: principles of CT and MRI interpretation. *Eur Radiol*. 2001; 11:1770–1783.
5. Hussain SM, Wielopolski PA, Martin DR. Abdominal magnetic resonance imaging at 3.0 T: problem or a promise for the future? *Top Magn Reson Imaging*. 2005;16:325–335.
6. Chang KJ, Kamel IR, Macura KJ, et al. 3.0-T MR imaging of the abdomen: comparison with 1.5 T. *Radiographics*. 2008;28: 1983–1998.
7. Akisik FM, Sandrasegaran K, Aisen AM, et al. Abdominal MR imaging at 3.0 T. *Radiographics*. 2007;27:1433–1444. discussion 1462, 1434.
8. Wehrli FW, Perkins TG, Shimakawa A, et al. Chemical shift–induced amplitude modulations in images obtained with gradient refocusing. *Magn Reson Imaging*. 1987;5:157–158.
9. Merkle EM, Nelson RC. Dual gradient-echo in-phase and opposed-phase hepatic MR imaging: a useful tool for evaluating more than fatty infiltration or fatty sparing. *Radiographics*. 2006; 26:1409–1418.
10. Mortelet KJ, Ros PR. Imaging of diffuse liver disease. *Semin Liver Dis*. 2001;21:195–212.
11. Holland HK, Spivak JL. Hemochromatosis. *Med Clin North Am*. 1989; 73:831–845.
12. Alústiza JM, Artetxe J, Castiella A, et al. MR quantification of hepatic iron concentration. *Radiology*. 2004;230:479–484.
13. Mergo PJ, Ros PR, Buetow PC, et al. Diffuse disease of the liver: radiologic-pathologic correlation. *Radiographics*. 1994; 14:1291–1307.
14. McLaren GD, Muir WA, Kellermeyer RW. Iron overload disorders: natural history, pathogenesis, diagnosis, and therapy. *Crit Rev Clin Lab Sci*. 1983; 19:205–266.
15. Schneider GnMD, Grazioli L, Saini S. *MRI of the Liver: Imaging Techniques, Contrast Enhancement, Differential Diagnosis*. 2nd ed. Milan, Italy: Springer; 2006.
16. Dolbey CH. Hemochromatosis: a review. *Clin J Oncol Nurs*. 2001;5: 257–260.
17. Lwakatare F, Hayashida Y, Yamashita Y. MR imaging of hepatocellular carcinoma arising in genetic hemochromatosis. *Magn Reson Med Sci*. 2003;2:57–59.
18. Hernando D, Levin YS, Sirlin CB, et al. Quantification of liver iron with MRI: state of the art and remaining challenges. *J Magn Reson Imaging*. 2014;40:1003–1021.
19. Alústiza Echeverría JM, Castiella A, Emparanza JI. Quantification of iron concentration in the liver by MRI. *Insights Imaging*. 2012; 3:173–180.
20. Campo CA, Hernando D, Schubert T, et al. Standardized approach for ROI-based measurements of proton density fat fraction and R2* in the liver. *AJR Am J Roentgenol*. 2017;209:592–603.
21. Beddy P, McCann J, Ahern M, et al. MRI assessment of changes in liver iron deposition post-venesection. *Eur J Radiol*. 2011;80:204–207.
22. Roubidoux MA. MR of the kidneys, liver, and spleen in paroxysmal nocturnal hemoglobinuria. *Abdom Imaging*. 1994;19:168–173.
23. Horowitz JM, Nikolaidis P, Chen ZM, et al. Iron deposition surrounding the hepatic veins of cirrhotic patients on MRI. *J Magn Reson Imaging*. 2011; 33:598–602.
24. Krinsky GA, Lee VS, Nguyen MT, et al. Siderotic nodules in the cirrhotic liver at MR imaging with explant correlation: no increased frequency of dysplastic nodules and hepatocellular carcinoma. *Radiology*. 2001;218:47–53.
25. Yu JS, Chung JJ, Kim JH, et al. Fat-containing nodules in the cirrhotic liver: chemical shift MRI features and clinical implications. *AJR Am J Roentgenol*. 2007;188:1009–1016.
26. Terada T, Nakanuma Y, Hosono M, et al. Fatty macroregenerative nodule in non-steatotic liver cirrhosis. A morphologic study. *Virchows Arch A Pathol Anat Histopathol*. 1989;415:131–136.
27. Kutami R, Nakashima Y, Nakashima O, et al. Pathomorphologic study on the mechanism of fatty change in small hepatocellular carcinoma of humans. *J Hepatol*. 2000;33:282–289.
28. Kadoya M, Matsui O, Kitagawa K, et al. Segmental iron deposition in the liver due to decreased intrahepatic portal perfusion: findings at MR imaging. *Radiology*. 1994;193:671–676.
29. Buhl L, Muirhead DE, Prentis PF. Renal hemosiderosis due to thalassemia: a light and electron microscopy study with electron probe x-ray microanalysis. *Ultrastruct Pathol*. 1993;17:169–183.
30. Mulopulos GP, Turner DA, Schwartz MM, et al. MRI of the kidneys in paroxysmal nocturnal hemoglobinuria. *AJR Am J Roentgenol*. 1986; 146:51–52.
31. Hertz IH, Keller RJ. Paroxysmal nocturnal hemoglobinuria: small bowel findings. *AJR Am J Roentgenol*. 1981;136:204–205.
32. Tabbara IA. Hemolytic anemias. Diagnosis and management. *Med Clin North Am*. 1992;76:649–668.
33. Kim SH, Kim S, Lee JS, et al. Hemorrhagic fever with renal syndrome: MR imaging of the kidney. *Radiology*. 1990;175:823–825.
34. Jeong JY, Kim SH, Lee HJ, et al. Atypical low-signal-intensity renal parenchyma: causes and patterns. *Radiographics*. 2002;22:833–846.
35. Queiroz-Andrade M, Blasbalg R, Ortega CD, et al. MR imaging findings of iron overload. *Radiographics*. 2009;29:1575–1589.
36. Sahni VA, Mortelè KJ. The bloody pancreas: MDCT and MRI features of hypervascular and hemorrhagic pancreatic conditions. *AJR Am J Roentgenol*. 2009;192:923–935.
37. Adler DD, Glazer GM, Aisen AM. MRI of the spleen: normal appearance and findings in sickle-cell anemia. *AJR Am J Roentgenol*. 1986;147: 843–845.
38. Luna A, Ribes R, Caro P, et al. MRI of focal splenic lesions without and with dynamic gadolinium enhancement. *AJR Am J Roentgenol*. 2006;186: 1533–1547.
39. Sagoh T, Itoh K, Togashi K, et al. Gamna-Gandy bodies of the spleen: evaluation with MR imaging. *Radiology*. 1989;172:685–687.
40. Ito K, Mitchell DG, Honjo K, et al. MR imaging of acquired abnormalities of the spleen. *AJR Am J Roentgenol*. 1997;168:697–702.
41. Abbott RM, Levy AD, Aguilera NS, et al. From the archives of the AFIP: primary vascular neoplasms of the spleen: radiologic-pathologic correlation. *Radiographics*. 2004;24:1137–1163.
42. Winchester PH, Cerwin R, Dische R, et al. Hemosiderin laden lymph nodes. An unusual roentgenographic manifestation of homozygous thalassemia. *Am J Roentgenol Radium Ther Nucl Med*. 1973;118:222–226.
43. Jordan E, Poder L, Courtier J, et al. Imaging of nontraumatic adrenal hemorrhage. *AJR Am J Roentgenol*. 2012;199:W91–W98.
44. Adam SZ, Nikolaidis P, Horowitz JM, et al. Chemical shift MR imaging of the adrenal gland: principles, pitfalls, and applications. *Radiographics*. 2016;36:414–432.
45. Drakonaki E, Papakonstantinou O, Maris T, et al. Adrenal glands in beta-thalassemia major: magnetic resonance (MR) imaging features and correlation with iron stores. *Eur Radiol*. 2005;15:2462–2468.
46. Guzelbey T, Gurses B, Ozturk E, et al. Evaluation of iron deposition in the adrenal glands of β thalassemia major patients using 3-tesla MRI. *Iran J Radiol*. 2016;13:e36375.
47. Gougoutas CA, Siegelman ES, Hunt J, et al. Pelvic endometriosis: various manifestations and MR imaging findings. *AJR Am J Roentgenol*. 2000; 175:353–358.